47th AIAA Structures, Structural Dynamics and Materials Conference, May 1-4, 2006 Newport, Rhode Island

Comparative Analysis of Computational Methods for Limit-Cycle Oscillations

Arathi K. Gopinath*
Stanford University, Stanford, CA 94305-4035
Philip S. Beran†
Air Force Research Laboratory, Wright-Patterson AFB, OH 45433
and
Antony Jameson‡
Stanford University, Stanford, CA 94305-4035

Various methods are explored in the computation of time-periodic solutions for autonomous systems. The purpose of the work is to illuminate the capabilities and limitations of methods, including a new method developed as part of the work, not based on time integration for the fast computation of limit-cycle oscillations (LCO). Discussion will focus on methodology, robustness, accuracy, and frequency prediction. Results for a model problem are shown in which temporal discetization errors during LCO are taken to machine zero. Treatment of sharp transients during LCO is also discussed.

I. INTRODUCTION

A number of engineering problems fall into the category of time-periodic systems. Some of these applications are, stator-rotor combinations in turbomachinery, helicopter blades in forward flight, wind turbines, flapping flight, flow control using synthetic jets and limit-cycle oscillations. The numerical prediction of limit-cycle oscillations will be the focus of this paper.

Limit-cycle oscillation (LCO) is a limited-amplitude, self-sustaining oscillation produced by an aero-structural interaction. LCO results in an undesirable airframe vibration and limits the performance of the flight vehicle.

The prediction and alleviation of LCOs in air vehicles continues to be a challenge. State-of-the-art computational techniques for predicting LCO responses in aeroelastic systems still use time-integration methods which require a great deal of computational effort which translates into long turn-around times. These features make these methods not suitable for design optimization or routine use in the test and evaluation environment. The goal of the current work is to determine the range of applicability of models of varying fidelity to the numerical prediction of LCOs and the development of fast spectral methods for evaluating the dependence of LCOs on stochastic system parameters.

A cyclic method was developed to compute limit-cycle oscillations for potentially large, nonlinear, multi-disciplinary systems of equations.[1] To improve on this 2nd-order cyclic/finite difference method, two spectral based techniques are implemented. One is the time spectral method[2] developed at Stanford University which is along the lines of the harmonic balance method[3] developed at Duke University. These are algorithms that use a Fourier representation in time. The second method is the spectral element method[4,5] implemented here in a novel way for periodic systems in time.

*Doctoral Candidate, AIAA Student Member.

†Principal Research Aerospace Engineer, Multidisciplinary Technologies Center, Air Vehicles Directorate,AIAA Associate Fellow

‡Thomas V. Jones Professor of Engineering, Department of Aeronautics and Astronautics, AIAA Member

This paper will compare and contrast the three methodologies, their robustness, accuracy and frequency prediction capabilities. A simple model of an aeroelastic airfoil with nonlinear structural coupling will be used to demonstrate the efficacy of the procedure. In the final paper, a two-dimensional nonlinear panel will be considered.

II. Formulation

In this section, the mathematical formulation of the problem will be described. The cyclic method in combination with the finite difference method for the time discretization has been described in previous work.[1] The cyclic method will again be described here for clarity. Two other computational techniques, the Time Spectral method and the Spectral Element method will be used in conjunction with the cyclic method in place of the finite difference discretization.

A. Cyclic Method

Time-periodic solutions of the autonomous system

$$\frac{d\mathbf{x}}{dt} = \mathbf{f}(\mathbf{x}, \lambda)$$

are sought, where t is time, $\mathbf{x}(t)$ is an N_f-dimensional array of real variables, and f is an array of N_f nonlinear functions, dependent on $\mathbf{x}$ and a free parameter λ. The period of the response is denoted by T, such that

$$\mathbf{x}(t) = \mathbf{x}(t+T).$$

The time variable is scaled, $s \equiv t/T$, leading to an equation in which the period appears explicitly,

$$\frac{d\mathbf{x}}{ds} = T\mathbf{f}(\mathbf{x}, \lambda). \tag{1}$$

A set of points on the periodic orbit at N_t uniformly distributed time levels is selected, leading to an expanded set of $N_t N_f$ unknowns,

$$\mathbf{X} \equiv (\mathbf{X}_1, \mathbf{X}_2, ...\mathbf{X}_{N_t})^T = (\mathbf{x}(s_1), \mathbf{x}(s_2), ..., \mathbf{x}(s_{N_t}))^T,$$

where the subscript specifies the time level(i.e., $s_{j+1} = s_j + \Delta_s$; $\Delta_s = 1/N_t$).

Using the trapezoidal rule, (1) is descretized to yield an expanded collection of equations:

$$\mathbf{G}_j \equiv \frac{T}{2}(\mathbf{F}_{j+1} + \mathbf{F}_j) - (\frac{d\mathbf{X}}{ds})_j = 0 \qquad (j = 1, ..., N_t), \tag{2}$$

where $\mathbf{F}_j \equiv \mathbf{f}(x(s_j))$. The time derivative term $\frac{d\mathbf{X}}{ds}$ will be discretized using three different strategies and will be described in the later sections.

A closed set of equations,

$$\mathbf{G} \equiv (\mathbf{G}_1, \mathbf{G}_2, ..., \mathbf{G}_{N_t}, \mathbf{G}_{N_t+1}, \mathbf{G}_{N_t+2})^T = 0,$$

is obtained by adding a pair of scalar constraints to (2) that prevent the solution from being trivial (i.e. $\mathbf{X} = 0$ for all j):

$$\mathbf{G}_{N_t+1} \equiv (\mathbf{X}_j)_{k_1} - \beta_1 = 0, \tag{3}$$

$$\mathbf{G}_{N_t+2} \equiv (\mathbf{X}_j)_{k_2} - \beta_2 = 0, \tag{4}$$

where j is an arbitrary point on the cycle, usually taken to be 1, and k_1 and k_2 are indices corresponding to two different variables at that time instant. Constraint (3) is used to identify the "starting" point of the cycle, such that $\beta_1 = 0$ (assuming an oscillation approximately centered about 0 for the selected variable). Likewise, (4) is used to set the amplitude of the cycle, such that $\beta_2 \neq 0$. For the problem investigated herein, $k_1 = 1$ and $k_2 = 2$.

The addition of two equations is accompanied by an increase in the number of unknowns by 2. These unknowns are $\mathbf{X}_{N_t+1} \equiv \lambda$ and $\mathbf{X}_{N_t+2} \equiv T$. Thus, a total of $N_t N_f + 2$ equations are solved for not only the

LCO solution, but also the period of the oscillation and the value of the free parameter λ at which the LCO meets the amplitude constraint (4).

In symbolic form, the complete system of "cyclic" equations is expressed as

$$\mathbf{G}(\mathbf{X}) = 0, \tag{5}$$

where this system is solved for expanded form of $\mathbf{X}$,

$$\mathbf{X} = (\mathbf{X}_1, \mathbf{X}_2, ...\mathbf{X}_{N_t}, \lambda, T)^T.$$

System (5) is solved with Newton's method, and IMSL routines are used to carry out the matrix calculations. Typically, about 10 Newton iterates are required to satisfy $\mathbf{G} = 0$ to machine precision.

The Jacobian, $\mathbf{J}$ of the system is formulated numerically about some current solution approximation, $\mathbf{X}^\nu$, through one-sided approximations (ϵ_J is set to 10^{-6}):

$$[\mathbf{J}(\mathbf{X}^\nu)]_{i,j} \equiv \frac{1}{\epsilon_J}(\mathbf{G}_i(\mathbf{X}_j^\nu + \epsilon_J) - \mathbf{G}_i(\mathbf{X}_j^\nu)). \tag{6}$$

1. *Finite Difference Formulation*

The time derivative term is discretized using finite differences, so that,

$$(D_s\mathbf{X})_j \equiv (\frac{d\mathbf{X}}{ds})_j = \frac{\mathbf{X}_{j+1} - \mathbf{X}_j}{\Delta_s}.$$

Periodicity must be enforced in closing (5) at the end points. For the form of discretization described above, the last equation will take the form,

$$(D_s\mathbf{X})_{N_t} \equiv (\frac{d\mathbf{X}}{ds})_{N_t} = \frac{\mathbf{X}_1 - \mathbf{X}_{N_t}}{\Delta_s}.$$

With this modification, the time derivative operator takes the shape of a periodic-banded structure, i.e. a banded matrix with a wrap-around term.

2. *The Time Spectral Method*

The Time Spectral Method was originally proposed and validated in.[2] This method falls into the same category of algorithms called Harmonic Balance methods developed by K. Hall[3] from Duke University and Nonlinear Frequency Domain methods developed by McMullen et.al.[6,7] from Stanford University. This class of algorithms take advantage of the periodic nature of the problem, and use a Fourier representation in time. Whereas Harmonic Balance techniques use Fast Fourier Transforms(FFTs), the Time Spectral method works in the time domain by expressing the time-derivative operator as a matrix operator.

Recall that

$$\mathbf{X} = (\mathbf{X}_1, \mathbf{X}_2, ...\mathbf{X}_{N_t}, \lambda, T)^T$$

where

$$\mathbf{X}_1 = (x_1, x_2, x_3, ..., x_{N_f})_1,$$

i.e., $\mathbf{X}_1$ is an array of all points in the N_f-dimensional array at time level 1. Construct an array $\mathbf{w}$ which consists of one variable at all time levels.
The discrete fourier transform of $\mathbf{w}$, for a time period "1" (scaled time s has a period of 1), is given by

$$\hat{w}_k = \frac{1}{N_t}\sum_{n=0}^{N_t-1} w^n e^{-ik2\pi n\Delta_s}$$

and its inverse transform,

$$w^n = \sum_{k=-\frac{N_t}{2}}^{\frac{N_t}{2}-1} \hat{w}_k e^{ikn2\pi\Delta_s}, \tag{7}$$

where the time period is divided into N_t time intervals(N_t even), $\Delta_s = 1/N_t$.

From Eq.(7), the time discretization operator D_s can be written as

$$D_s w^n = 2\pi \sum_{k=-\frac{N_t}{2}}^{\frac{N_t}{2}-1} ik\hat{w}_k e^{ik2\pi n\Delta_s}.$$

This summation involving the fourier modes $\hat{w}_k$, can be rewritten in terms of w in the time domain, both for even and odd N_t as,[2,8,9]

$$D_s^{even} w^n = \sum_{m=-\frac{N_t}{2}+1}^{\frac{N_t}{2}-1} d_m^{even} w^{n+m},$$

and

$$D_s^{odd} w^n = \sum_{m=\frac{1-N_t}{2}}^{\frac{N_t-1}{2}} d_m^{odd} w^{n+m},$$

where

$$d_m^{even} = \begin{cases} \pi(-1)^{m+1}\cot(\frac{\pi m}{N_t}) & : \quad m \neq 0 \\ 0 & : \quad m = 0 \end{cases}$$

and

$$d_m^{odd} = \begin{cases} \pi(-1)^{m+1} cosec(\frac{\pi m}{N_t}) & : \quad m \neq 0 \\ 0 & : \quad m = 0 \end{cases}$$

Note that $d_{-m} = -d_m$ for both even and odd N_t. Hence D_s takes the form of a central difference operator connecting all the time levels, yielding an integrated space-time formulation which requires the simultaneous solution of the equations for all time levels.

Since the computation of D_s involves terms at all the time levels (i.e., full stencil), the time derivative matrix operator is full, which is typical of spectral methods. And since spectral methods use global basis functions in the form of sines and cosines, periodicity need not be explicitly imposed.

3. Spectral Element Formulation

Polynomial nodal expansions are based upon the Lagrange polynomials which are associated with a set of nodal points. The location of these nodal points in the domain play an important part in the stability of the approximation and the conditioning of the system. Using nodal points at the zeros of the Gauss-Legendre-Lobatto integration rule produces an efficient expansion which does not exhibit the oscillations seen when equi-spaced points are chosen. This class of nodal p-type elements are called spectral elements due to Patera.[4]

In this section, the formulation of the spectral element method for the system (1) will be presented. First, multiply equation (1) by the test function $v(s)$ and integrate over the orbit,

$$\oint v(s)\frac{dw}{ds}ds = \oint v(s)Tf(w(s))ds.$$

Using periodicity and the chain rule, rewrite as,

$$-\oint w(s)\frac{dv}{ds}ds = T\oint v(s)f(w(s))ds.$$

Since the entire orbit/domain is divided into a number of elements, consider the integral in each element,

$$-\int_{\Omega_j} w_j(s)\frac{dv_j}{ds}ds = T\int_{\Omega_j} v_j(s)f_j(w(s_j))ds,$$

using $v_j(s) = \phi_j$

$$T \int_{\Omega_j} \phi_j^p f_j(w(s_j))ds + \int_{\Omega_j} w_j(s) \frac{\partial \phi_j^p}{ds} ds = 0.$$

Using a change of variables, $s = s_j + \frac{\psi+1}{2}(s_{j+1} - s_j)$, rewrite as

$$T \int_{-1}^{1} \phi_j^p(\psi) f_j(w(\psi)) \frac{ds}{d\psi} d\psi + \int_{-1}^{1} w_j(\psi) \frac{d\phi_j^p}{d\psi} d\psi = 0$$

This equation is integrated using Gauss quadrature. Since the orbit is divided into sub-intervals, the time derivative in each sub-interval is directly dependent only on the points in its own sub-interval. In this way, some level of sparsity is retained, at the same time, high accuracy is ensured by using high-order polynomials within each sub-interval. Periodicity is enforced during global assembly by wrapping around the first and last elements.

III. Current Results

A. The Airfoil Problem

The aeroelastic system studied here is a nonlinear symmetric airfoil in low-speed flow, described by two physical DOFs: pitch and plunge.In the current study, a fifth-order element is added to the pitch restoring force, in addition to the third-order stiffness investigated previously.[10] The plunge DOF has linear stiffness but the pitch DOF includes a third-order and fifth-order stiffness terms in addition to the linear component. Hence, the restoring force associated with the torsional spring is expressed as $K_\alpha(\alpha + k_3\alpha^3 + k_5\alpha^5)$, where K_α is the dimensional linear stiffness and k_3 and k_5 are the dimensionless parameters governing the third- and fifth- order nonlinearities respectively. The free parameter λ, is defined to be a nondimensional parameter proportional to flight speed ("reduced velocity"), which when sufficiently large, leads to flutter or LCO responses of the system. The airfoil dynamics are represented by a system of eight ODEs, obtained through linear modeling of the aerodynamics.[10] The final form of the 8-DOF system is given in .[11] The details of the Hopf bifurcation can be found in.[1] A typical LCO branch is shown Figure 1.

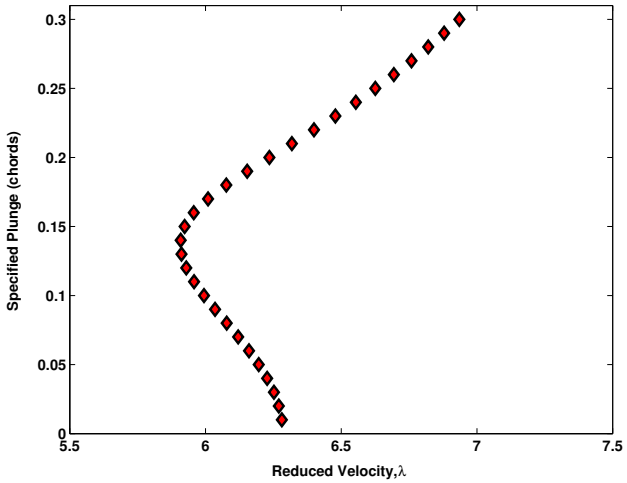

Figure 1. An LCO branch showing subcritical Hopf bifurcation

The computation of cyclic solutions requires the specification of initial conditions for the iterative process. Time integrations of system response in pitch and plunge revealed a clock-wise rotation of the phase portrait in these two parameters (pitch plotted on the abscissa). An initial approximation to the LCO dynamics was

imposed by assuming a circular trajectory in pitch and plunge, using the target cross-over value of plunge (β_2) to set the LCO amplitude.

The parameters governing the LCO are a specified plunge value (β_2) at a vanishing angle of attack (β_1). Plunge values are reported in nondimensional form, using airfoil chord as a scale factor. The torsional spring parameters k_3 and k_5 are specified to be -3 and 20, respectively, to produce a subcritical Hopf bifurcation.[12]

Figure 2(a) and (b) show comparisons of LCO branches in terms of specified values of β_2 for selected number of scaled time intervals per cycle (N_t) using finite difference method and time spectral method respectively. Note that as β_2 decreases, the LCO response weakens. The selection of N_t=100 leads to LCOs well converged in time step over most of the range in β_2 for the finite difference case. Whereas the time spectral method captures the LCO branch over the entire range of β_2 with just 40 scaled time intervals, to plotting accuracy.

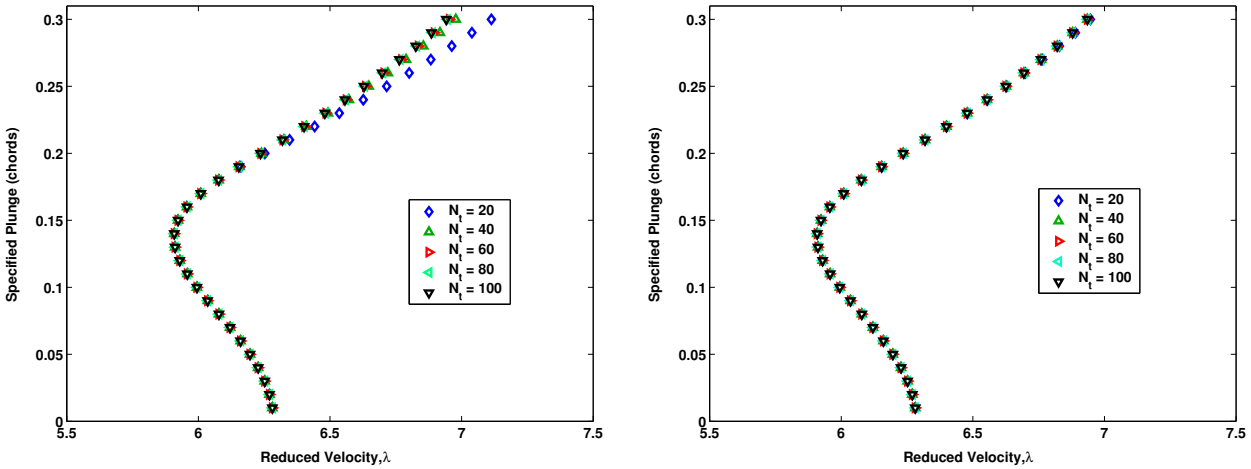

(a) Finite Difference (b) Time Spectral method

Figure 2. Comparison of LCO branches in terms of specified β_2 for selected numbers of scaled time steps per cycle(N_t) using Finite Difference and Time Spectral methods

A strong nonlinear response is observed beyond the subcritical Hopf bifurcation point computed at about $\lambda = 6.29$. This is further illustrated in Figure 3 and 4. Figure 3(a) shows the LCO(pitch vs. plunge), (b) shows the initial and final solution of variation of pitch as a function of scaled time and (c) the initial and final solution of plunge, computed at $\beta_2 = 0.3$ and $\lambda = 6.9351$.

Similarly, the phase-plane plots for $\beta_2 = 0.015$, a point close to the cyclic fold, are shown in Figure 4. This point shows a weaker response and hence requires fewer time intervals for high accuracy. The pitch and plunge also show a "sine"-like behavior which can be captured with fewer frequencies. Whereas for the strong nonlinear response point, the pitch curve shows a marked asymmetry and a variation unlike a "sine" function. These also transform into sharp-transients in the LCO plots, moving away from the "ellipse"-like structure. These characteristics require larger number of time intervals or DOF to be captured to high accuracy. Spectral based techniques with their high-order polynomial formulation have the ability to capture these features with smaller DOFs.

Figure 5 shows the log-log error ($T - T_c$) plot with refinement in N_t computed with the 3 different computational techniques for the strong nonlinear response point, $\beta_2 = 0.3$. Here T_c is the time period computed with 200 time intervals per cycle with the time spectral method. The convergence of the cyclic/FD method is verified to be second-order(algebraic convergence). Convergence of the cyclic/time spectral method using odd number of N_t shows near exponential convergence. Cyclic/time spectral algorithm shows machine precision accuracy with just 70 DOFs. Cyclic/spectral element h-extension (increasing number of elements, keeping P fixed, P=2) also shows algebraic convergence. A p-extension (increasing order of polynomial P, keeping number of elements fixed, $N_t = 2$), shows close to exponential convergence.

Similarly, Figure 6 shows the log-log error plot for a weaker LCO point, $\beta_2 = 0.15$. Convergence rates are very similar to the strong response point, but the cyclic/time spectral method converges to machine precision using only 40 DOFs. As explained earlier, this is attributable to the fact that the frequency content in this case is lower, as shown in Fig 4. Also, for small number of DOF ($N_t < 10$), this case shows smaller error

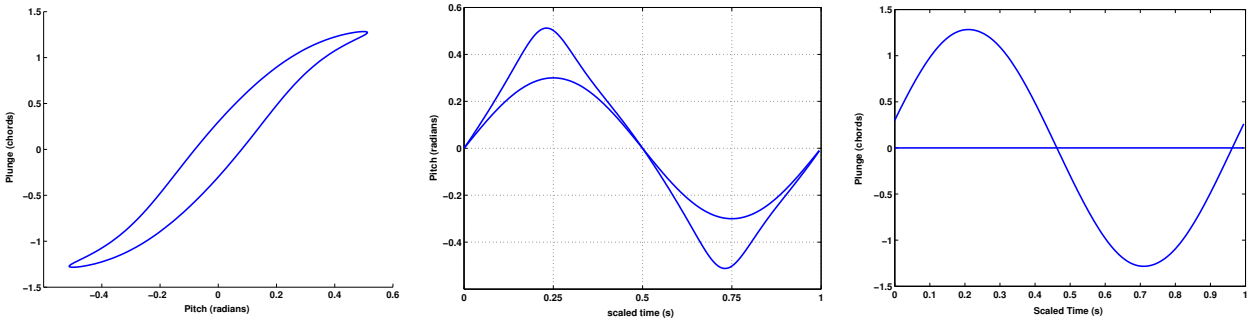

(a) LCOs (b) Time history of pitch (c) Time history of plunge

Figure 3. Phase-plane plots computed for $\beta_2 = 0.3$(initial and final iterate of pitch and plunge shown)

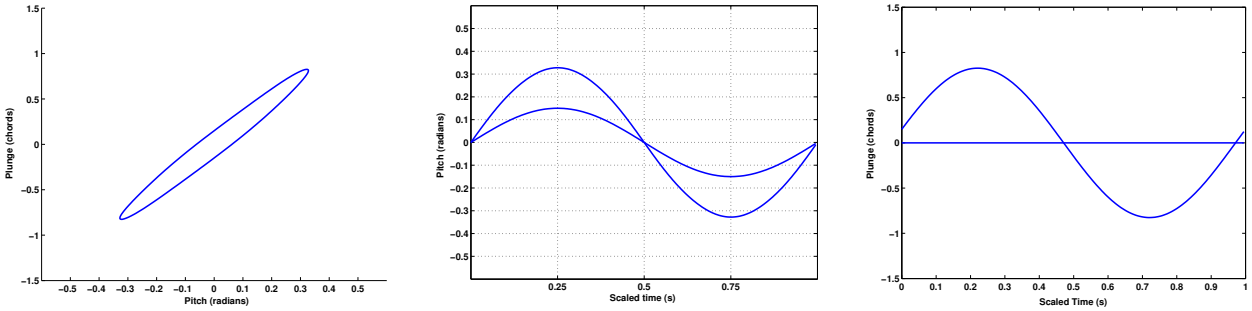

(a) LCOs (b) Time history of pitch (c) Time history of plunge

Figure 4. Phase-plane plots computed for $\beta_2 = 0.15$(initial and final iterate of pitch and plunge shown)

compared to the $\beta_2 = 0.3$ case.

IV. Conclusions and Future Work

Two spectral based computational techniques were implemented in combination with the cyclic method for the numerical prediction of LCOs. As expected, the finite difference method showed algebraic convergence. The time spectral method based on global basis functions captured rapid-transients with few DOF, but could prove to be prohibitive for big systems since it produces full matrices. On the other hand, the spectral element method showed good promise with respect to accuracy and has the potential for *hp* convergence. It produces sparse matrices and uses high-order polynomials to ensure high accuracy.

We propose to include the following attributes in the final paper:

- The cyclic/spectral element method has the capability to be made adaptive in regions of steep-transients where higher resolution might be required. Implement a strategy for defining spectral elements of unequal sub-intervals in time.
- A simple aeroelastic model of an airfoil with nonlinear structural coupling was used to show the efficacy of the procedure in this abstract. Use a more challenging problem like a 2D nonlinear panel in high speed flow and study the capabilities and limitations of the various techniques.
- Improve the efficiency of the numerical formulations, especially the iterative process which currently takes up most of the CPU time.

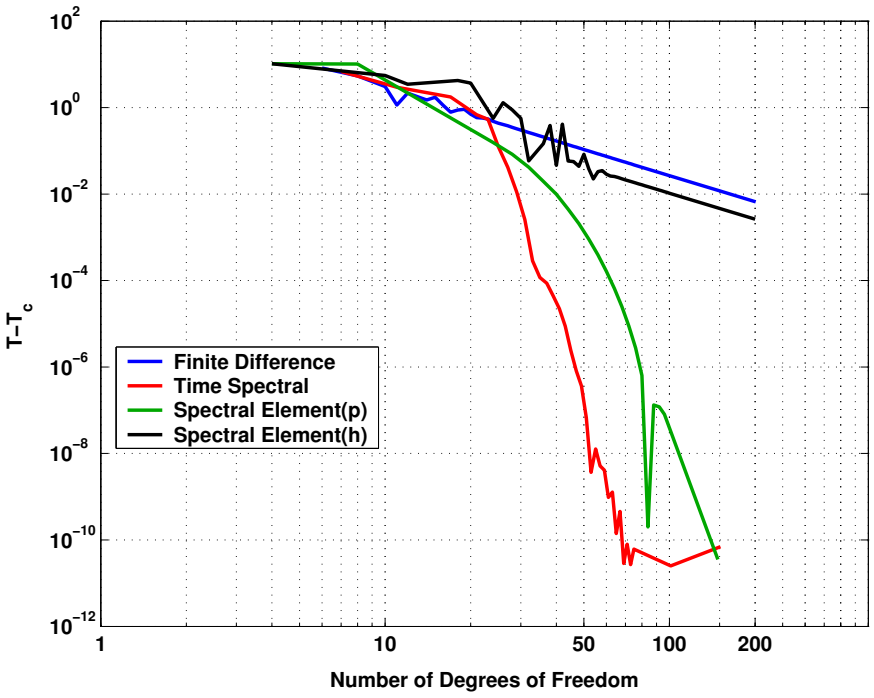

Figure 5. Computed time period error plot using the three different computational methods for $\beta_2 = 0.3$

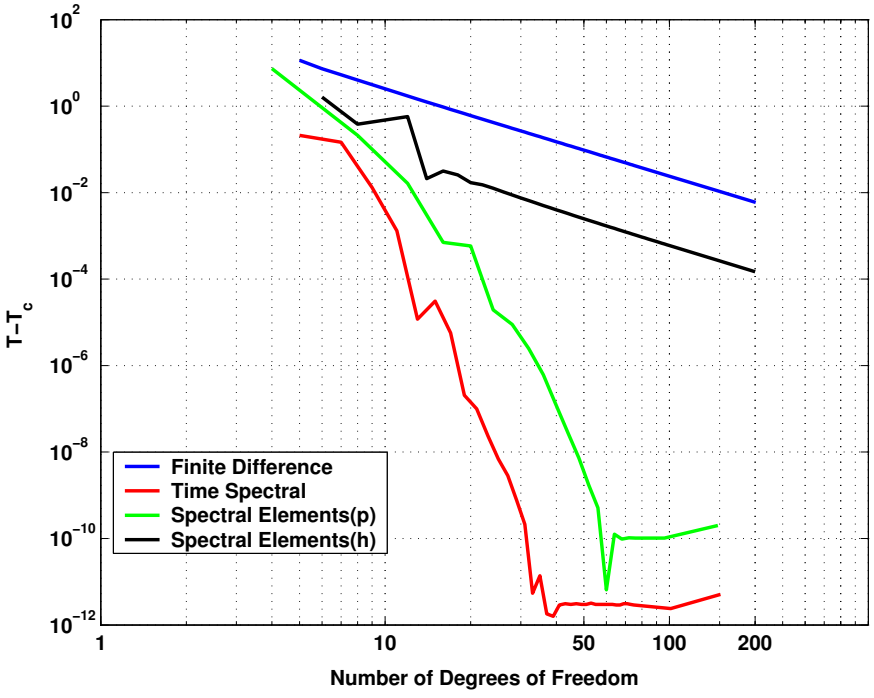

Figure 6. Computed time period error plot using the three different computational methods for $\beta_2 = 0.15$

V. Acknowledgement

The authors would like to thank the Air Force Office of Scientific Research (Dr. Fariba Fahroo, PM) for the support of this work through LRIR 03VA01COR.

References

[1]P.S. Beran and D.J. Lucia. A reduced order cyclic method for computation of limit cycles. *Nonlinear Dynamics*, 39:143–158, 2005.

[2]A. Gopinath and A. Jameson. Time spectral method for periodic unsteady computations over two- and three-dimensional bodies. *AIAA paper 05-1220*, AIAA 43rd Aerospace Sciences Meeting and Exhibit, Reno, NV, January 10-13 2005.

[3]K.C. Hall, J.P. Thomas, and W.S. Clark. Computation of unsteady nonlinear flows in cascades using a harmonic balance technique. *AIAA Journal*, 40(5):879–886, May 2002.

[4]A.T. Patera. A spectral method for fluid dynamics: Laminar flow in a channel expansion. *J. Computational Physics*, (*54:468*), 1984.

[5]G.E. Karniadakis and S.J. Sherwin. *Spectral/hp Element Methods for CFD*. Oxford University Press, 1999.

[6]M. McMullen, A. Jameson, and J.J. Alonso. Acceleration of convergence to a periodic steady state in turbomachinery flows. *AIAA paper 01-0152*, AIAA 39th Aerospace Sciences Meeting, Reno, NV, January 2001.

[7]M. McMullen, A. Jameson, and J.J. Alonso. Application of a non-linear frequency domain solver to the euler and navier-stokes equations. *AIAA paper 02-0120*, AIAA 40th Aerospace Sciences Meeting and Exhibit, Reno, NV, January 2002.

[8]A. Quarteroni C. Canuto, M.Y. Hussaini and T.A. Zang. *Spectral Methods in Fluid Dynamics; Springer Series in Computational Physics*. Springer Verlag, 1988.

[9]E. Van der Weide, A. Gopinath, and A. Jameson. Turbomachinery applications with the time spectral method. *AIAA paper 05-4905*, 17th AIAA Computational Fluid Dynamics Conference, Toronto, Ontario, June 6-9 2005.

[10]B. Lee, L. Jiang, and Y. Wong. Flutter of an airfoil with a cubic restoring force. *AIAA*, 1998-1725, April 1998.

[11]D.R. Millman, P.I. King, and P.S. Beran. A stochastic approach for predicting bifurcation of a pitch and plunge airfoil. *AIAA*, 2003-3515, June 2003.

[12]C.L. Pettit and P.S. Beran. Effects of parametric uncertainty on airfoil limit-cycle oscillation. *Journal of Aircraft*, 40(5):1004–1006, Sep-Oct 2003.